Neuron
Article

A Predictive Network Model of Cerebral Cortical Connectivity Based on a Distance Rule

Mária Ercsey-Ravasz,[1,2,8] Nikola T. Markov,[3,4,5,8] Camille Lamy,[3,4] David C. Van Essen,[6] Kenneth Knoblauch,[3,4,9] Zoltán Toroczkai,[1,7,9,*] and Henry Kennedy[3,4,9,*]
[1]Department of Physics and Interdisciplinary Center for Network Science and Applications, University of Notre Dame, Notre Dame, IN 46556, USA
[2]Faculty of Physics, Babeş-Bolyai University, 400084 Cluj-Napoca, Romania
[3]Stem Cell and Brain Research Institute, INSERM U846, 69500 Bron, France
[4]Université de Lyon, Université Lyon I, 69003 Lyon, France
[5]Department of Neurobiology, Yale University, New Haven, CT 06520, USA
[6]Department of Anatomy and Neurobiology, Washington University School of Medicine, St. Louis, MO 63110-1093, USA
[7]Max Planck Institute for the Physics of Complex Systems, 01187 Dresden, Germany
[8]These authors contributed equally to this work
[9]These authors contributed equally to this work
*Correspondence: toro@nd.edu (Z.T.), henry.kennedy@inserm.fr (H.K.)
http://dx.doi.org/10.1016/j.neuron.2013.07.036

SUMMARY

Recent advances in neuroscience have engendered interest in large-scale brain networks. Using a consistent database of cortico-cortical connectivity, generated from hemisphere-wide, retrograde tracing experiments in the macaque, we analyzed interareal weights and distances to reveal an important organizational principle of brain connectivity. Using appropriate graph theoretical measures, we show that although very dense (66%), the interareal network has strong structural specificity. Connection weights exhibit a heavy-tailed lognormal distribution spanning five orders of magnitude and conform to a distance rule reflecting exponential decay with interareal separation. A single-parameter random graph model based on this rule predicts numerous features of the cortical network: (1) the existence of a network core and the distribution of cliques, (2) global and local binary properties, (3) global and local weight-based communication efficiencies modeled as network conductance, and (4) overall wire-length minimization. These findings underscore the importance of distance and weight-based heterogeneity in cortical architecture and processing.

INTRODUCTION

A characteristic feature of the cerebral cortex is its modular organization. Sensory, motor, and cognitive systems are organized as constellations of distinct areas, each within a well-defined region or lobe. Analyses of the functional specificities of individual areas and of their cooperative and competitive interactions mediated by numerous interareal pathways have provided profound insights concerning the role of the cortex in higher functions (Mountcastle, 1998; Schüz and Miller, 2002; Zeki, 2005). Anatomical tract-tracing methods permit the analysis of cortical connectivity at much higher resolution than is currently possible with in vivo brain imaging techniques (Bakker et al., 2012; Lanciego and Wouterlood, 2011). Numerous tracer studies have extensively characterized the pathways linking cortical areas and have revealed many important principles of organization (Aflalo and Graziano, 2011; Barbas and Rempel-Clower, 1997; Boussaoud et al., 1990; Felleman and Van Essen, 1991; Jouve et al., 1998; Kaas and Collins, 2001; Rockland, 1997; Rosa and Tweedale, 2005; Sporns et al., 2000; Vezoli et al., 2004; Young, 1992; Zeki and Shipp, 1988). Nevertheless, many fundamental aspects of cortical circuitry remain poorly understood (Bohland et al., 2009; Van Essen and Ugurbil, 2012).

Our current understanding of cortical connectivity owes much to the seminal work of Sporns and coworkers who conceptualized interareal neuroanatomy in terms of graph theory (Sporns et al., 2000). The fundamental motivation is that the analyses of the network properties of complex systems can provide insights into the computations that they carry out (Barabasi and Albert, 1999; Boccaletti et al., 2006; Newman, 2003; Watts, 1999b; Watts and Strogatz, 1998). Investigation of the cortical graph has made important progress, showing for instance that the brain exhibits a remarkable economy in its organization (Bullmore and Sporns, 2012; Sporns, 2011). Further, studies using subgraphs with low densities suggest that cortical networks are structurally heterogeneous, exhibiting a highly connected core region (high centrality) that may provide an important integrative capacity to the cortex (Harriger et al., 2012; Modha and Singh, 2010; van den Heuvel et al., 2012).

The data sets used in early investigations of the structural organization of the cortical network at the single-cell level largely relied on data that were based on binary (yes/no) assessments of connectivity and were collated across numerous experimental

studies. While this approach has been highly productive, it has inherent limitations due to inconsistencies between laboratories as well as the use of incomplete and nonquantitative data (Kennedy et al., 2013).

A recent study set out to establish a consistent database of interareal connectivity using sensitive retrograde tracers in order to determine the weighted connectivity of the inputs to 29 areas in an atlas of 91 cortical areas (Markov et al., 2012). This large-scale anatomical investigation of the macaque cortex provided a weighted and directed connectivity matrix in which the 29 injected areas are linked by 1,615 interareal pathways. Over one-third of these pathways had not been reported in previous studies. While a single injection only provides information about the inputs to a given area, the set of 29 injections provides a complete assessment of the inputs and outputs within the subgraph of 29 areas (G_{29x29}). Such *edge-complete* subgraphs of a large network are expected to possess many of the properties of the network from which they are extracted. In particular, because the 29 injections are widely distributed within the full set of 91 cortical areas, it is expected that the properties of the G_{29x29} subgraph are representative of the full interareal network (FIN). Note that this is not typically the case for subgraphs based on edge-incomplete data.

Analysis of the G_{29x29} subgraph revealed a number of unexpected network properties (Markov et al., 2013). Foremost, the cortical graph has a much higher density (66% of the connections that can exist do exist) than expected from previous work on collated databases. If connections were homogenously spread across the cortex, such a high density would preclude significant binary specificity within the graph. However, the probability of a connection existing between any two given areas declines sharply with distance (Markov et al., 2013). This explains the observed specificity of long-range between-lobe connections, which is directly related to the spatial embedding of the network. By contrast, within-lobe connections were shown to exhibit low binary specificity, since nearly all the possible connections actually occur (i.e., densities approach 100%). These results suggest that the cortico-cortical connections within the constellation of areas of a particular lobe or region achieve their specificity mainly via the heterogeneity of their weights (Markov et al., 2011, 2012).

Contrary to some virtual networks such as the world-wide web, the cortical network is a spatially embedded physical network. It is constructed under evolutionary pressure acting on physical parameters, such as wire length and overall network volume, that impose constraints on its architecture. Such evolutionary pressure could mean that wire length minimization will impose constraints on network connectedness with increasing brain size (Ringo, 1991). Indeed, there is evidence that the structure and function of cortical networks optimize resources and satisfy constraint minimization at multiple scales, thereby influencing diverse aspects of cortical architecture including arealization and cortical folding (Chklovskii and Koulakov, 2004; Klyachko and Stevens, 2003; Laughlin and Sejnowski, 2003; Mitchison, 1991; Rivera-Alba et al., 2011; Van Essen, 1997). In order to quantitatively assess the role of wire minimization on the cortical architecture, we estimated the numbers of wires (i.e., number of cells projecting onto an injection site yielding the strength or weight of connection) between areas and the distance of projections (see Experimental Procedures).

As noted above, interareal distances play an important role in defining certain aspects of the specificity of the cortical graph, meaning that its embedded nature (i.e., its spatial organization) must be taken into consideration. However, given the high density of the G_{29x29} graph, appropriate graph theoretic approaches must also be used. Three features of the data concerning weight and distance have governed our approach: first, the weights of the pathways span five orders of magnitude; second, weights are distributed in a lognormal fashion; and third, interareal distances are normally distributed (Markov et al., 2011, 2012, 2013).

Here, we examine how multiple aspects of our data interact to predict important features of cortical organization and, by implication, the information theoretical function therein. We demonstrate that important graph theoretical characteristics of the cortical network, as well as its previously reported specificity (Markov et al., 2013) and core-periphery structure (Harriger et al., 2012; Modha and Singh, 2010), can be formulated in terms of a wiring economy principle (quantified as an exponential distance rule) with the help of a single-parameter network model. This unique, physical parameter expresses the decline in the probability of axonal projection as a function of distance and is extracted from anatomical data. The implications of these findings are considered in the Discussion.

RESULTS

Connection weights were derived from a connectivity matrix based on interareal connection strengths in the macaque (Markov et al., 2012). The weight of a projection from a source area to a given target area (the area injected) is defined by the fraction of labeled neurons (FLN) expressed as the ratio between the number of labeled neurons in that source area over the total number of labeled cortical neurons extrinsic to the injected area. Distances were measured as the length of the shortest trajectory interconnecting areas via the white matter, approximating the axonal distance (see Supplemental Information available online).

A Spatially Embedded and Weighted Network

The projections between the $N_F = 91$ areas comprise the full interareal network (FIN), which is a directed, weighted, spatially embedded graph G_{91x91} on 91 nodes. The FLN f_{ij} of a link projecting from area i to area j represents the weight of that projection (later parameterized as $w_{ij} = -\log f_{ij}$, for a conductance-type analysis). The n = 29 injections have identified a total of E = 1,615 edges of G_{91x91}, forming the currently known subgraph G_{29x91} of FIN. The 29 × 29 directed graph G_{29x29} includes only the injected areas and their interconnections, and therefore it has *full connectivity* information within this set. Accordingly, G_{29x29} is an edge-complete subgraph of the FIN. Given that injected areas are evenly distributed across the cortex, the statistical properties of G_{29x29} are likely to be representative of the FIN. The G_{29x29} subgraph has M = 536 (binary) links out of the maximum possible of $N(N-1)$ = 812; it is a very dense graph with a density $(\rho = M/[N(N-1)])$ of 66% (Markov et al., 2012).

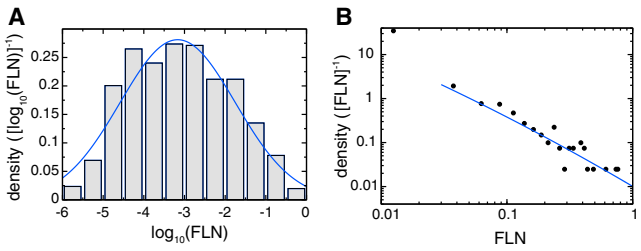

Figure 1. Distribution of the Pooled Fraction of Labeled Neurons for the 29 Target Areas

(A) FLN values span five orders of magnitude and follow a lognormal distribution in this density plot. Log_{10}(FLN) values were binned (bin size 0.5), the height of each bin (ordinate) corresponds to the fraction of projections with log_{10}(FLN) falling within that bin divided by the bin width. Blue, Gaussian fit with mean at $\mu_{Gauss} = -3.17$ (location parameter) and SD of $\sigma_{Gauss} = 1.42$ (scale parameter), both in units of log_{10}(FLN).

(B) Right tail (large FLN values) of the distribution exhibits a slow, power-law decay as shown by the double logarithmic plot. Blue line in (B), right tail of the lognormal in (A). This is also a density plot, as in (A). In this case, the binning was done directly on the FLN values with a bin width of 0.025 FLN. With this choice for bin width, the right tail of the distribution is formed by those high FLN values that fall outside of one sigma ($\sigma_{Gauss} = 1.42$) in (A).

A Distance Rule as a Cost-of-Wiring Principle

For each injected area, the distribution of FLNs (incoming link weights) is lognormal (Markov et al., 2011, 2012). Figure 1A shows that the pooled distribution of FLN values for all the 29 injections also has a lognormal distribution, hence exhibiting a heavy tail (Figure 1B). Here we show that the FLN decays exponentially as a function of projection distance. This allows formulation of a global distance rule as a principle of allocation of resources in the cortex. Figure 2A shows the log(FLN) values for all 1,615 projections of G_{29x91} as a function of interareal projection length. In spite of the variability in the data, there is a clear decay trend (red, linear fit) with increasing distance. However, the FLNs group neuronal counts via the injected areas, thus providing a binning by areas. Projections at longer distances come at a metabolic cost for individual neurons. To better express this cost principle as a global (area-independent) property, Figure 2B shows a histogram for all retrogradely labeled neurons found from the 29 injections (a total of 6,494,974) as function of the projection distance between cortical areas. This exhibits an exponential decay that we refer to as the "exponential distance rule" (EDR). Accordingly, *p(d)* can be interpreted as the probability of a projection length *d*, irrespectively of the areas involved. Based on Figure 2B, we express this principle as:

$$p(d) = c\,\exp(-\lambda d) \tag{1}$$

where *c* is a normalization constant and $\lambda = \lambda_d = 0.188$ mm^{-1} (obtained from least-squares fitting, Figure 2B). The blue line in Figure 2A corresponds to Equation (1) with $\lambda = \lambda_d$, indicating that it is a good approximation for the linear decay trend (red line with $\lambda_{f_{ij}} = 0.150$ mm^{-1} in Figure 2A) of the log(FLN) values as well. Since the fraction of labeled neurons f_{ij} can be interpreted as the probability of a neuronal projection from *i* to *j*, the agreement in Figure 2A shows that, on average, we can approximate the FLN values with their distance-dependent projection probabilities, i.e., $f_{ij} \approx p(d_{ij}) = ce^{-\lambda d_{ij}}$, where d_{ij} is the distance between the areas. From this, the distance between two areas can on average be expressed in terms of the corresponding log(FLN) values (natural log) as:

$$d_{ij} \approx -\frac{1}{\lambda}\log f_{ij} + \frac{1}{\lambda}\log c. \tag{2}$$

The distribution of the interareal distances (i.e., the fraction of area pairs separated by distance *d*) conforms to a Gaussian (see Figure 2C), i.e.,

$$q(d) = \frac{1}{\sigma\sqrt{2\pi}}\exp\left[-\frac{1}{2\sigma^2}(d-\mu)^2\right], \tag{3}$$

with $\mu = 26.57$ mm and $\sigma = 10.11$ mm. Note that Equation (3) expresses a *geometrical property* of the cortex, the distribution of areal separations, and is not related to neuronal counts or densities. Substituting the distance variable in Equation (3) with its expression in terms of log(FLN)s from Equation (2), gives an approximation to the fraction of ordered area pairs that have a given log(FLN) value, i.e., an approximation to the log(FLN) distribution:

$$P(\log(f)) = q(d(f)) = \frac{\lambda}{\gamma\sqrt{2\pi}}\exp\left[-\frac{1}{2\gamma^2}(\log f - \nu)^2\right] \tag{4}$$

with $\gamma = \sigma\lambda$ and $\nu = \mu\lambda - \log c$. This is indeed a Gaussian, consistent with the experimental observation that the FLN distribution is a lognormal. Note that this derivation captures only the lognormal form, as we have replaced distances in Equation (3) by an expression of the FLNs that holds only on average, Equation (2). Accordingly, the width of the Gaussian distribution in Figure 1A (data) is wider than that of Equation (4), due to fluctuations around the average.

An EDR-Based Network Model of the Cortex

Because the G_{29x29} graph is a densely connected network, one might expect there to be little structural specificity on the binary level (nodes connected or not). However, G_{29x29} is actually a special graph even at the binary level. This specificity follows directly from the EDR (decreasing probability of projection with distance principle), acting as a *physical* constraint and the spatial embedding of the cortex acting as a *geometrical* constraint. To explore further the role of distance in the structural properties of the cortical network, we generated two random graph models using different distance rules. One obeys the observed exponential distance rule (1) (EDR graphs), the other a constant distance rule $p(d) = const$, in which the probability of a projection having a distance *d* is a constant (CDR graphs). The CDR model can be considered a special case of EDR with λ = 0. To construct the model graphs, we first chose a connection length *d* according to the distance rule *p(d)*. We next pick *uniformly at random* (to avoid biases, following Jaynes' maximum entropy principle; Jaynes, 1957) an area pair (*i,j*) from the set of area pairs in the 29 × 29 matrix of measured distances, whose separation is in the same distance bin as *d*, then insert a connection in the graph directed from *j* to *i*. Multiple connections from *j* to *i* are allowed, thus generating the projection's *weight*; the process is halted after accumulating *M* = 536 *binary connections* (i.e., the number

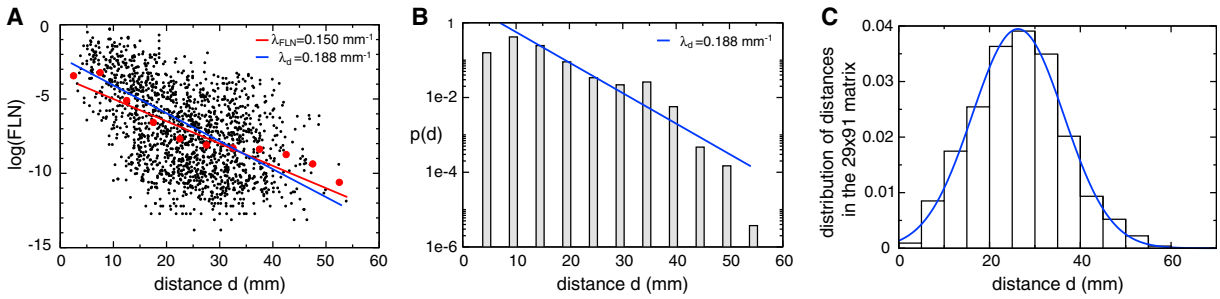

Figure 2. Projection Length Distributions in the Macaque Cortex

(A) FLN values (log f_{ij}) for all 1,615 projections as a function of projection length (d_{ij}) estimated through the white matter. Red circles, averages within 5 mm distance bins; the red line is an exponential fit to all the black points giving a decay rate of $\lambda_{FLN} = 0.150$ mm^{-1}.

(B) Histogram of interareal projection length for all labeled neurons (n = 6,494,974). Blue line, exponential fit with decay rate $\lambda_d = 0.188$ mm^{-1}, also shown in (A).

(C) Distribution of interareal distances in G_{29x91} matrix, a purely geometrical property, is best approximated by a Gaussian (mean $\langle d \rangle = \mu = 26.57$ mm; SD $\sigma = 10.11$ mm).

of connections in the G_{29x29}). To compare graph theoretical properties between the model and the cortical graph G_{29x29}, we generated 1,000 random realizations of each model graph, averaged the measured quantity over these realizations, and compared this average to the same measure on G_{29x29}.

Prediction of Frequency of Uni- and Bidirectional Connections

Previous studies of collated data had suggested that connections between cortical areas are dominated by reciprocally interconnected pathways (Felleman and Van Essen, 1991). Markov et al. (2013) reported a higher incidence of unidirectional, nonreciprocal connections. Here we show that this feature is well captured by the EDR. If M_1 and M_2 are the number of uni- and bidirectional connections, respectively, the total is $M = M_1 + 2M_2$. The simplest quantity that we can compare between model and data graphs is the total number of unidirectional connections M_1 (because M is specified, M_2 is automatically determined). Varying λ modulates the distribution of M_1 and M_2, see Figure 3A. Since λ is the only model parameter, we set it to $\lambda = \lambda_M \cong 0.174$ mm^{-1} (Figure 3A) so that $\langle M_1 \rangle(\lambda) = M_1 = 108$, the reported number of unidirectional connections (Markov et al., 2012). Thus, λ_M is set by a purely binary graph theoretical measure of the data, not by weights, distances, or neuronal counts, yet it agrees closely with the decay rate $\lambda_d = 0.188$ mm^{-1}, obtained from the histogram of projection lengths of Figure 2B. This agreement stems from the fact that the EDR rule is a strong determinant of the cortical network structure (see below).

Prediction of Motif Distribution

A basic binary characteristic of a directed network is its frequency distribution of directed small binary subgraphs that can be considered as network building blocks that are characteristic of different types of networks (Milo et al., 2002). For example, Milo et al. (2002) looked at three-node motifs and showed that information-processing networks were characterized by certain, abundant triangular motifs. There are 16 possible three-node motifs (abscissa symbols in Figures 3B and 3C). The EDR model returns motif frequencies similar to those found in the data as shown in Figure 3B. Figure 3C compares the deviations by considering the log of the ratio of the model motif count to the count of the same motif in the data. Let σ_Δ denote the SD of the fluctuations in Figure 3C. Figure 3D plots σ_Δ versus λ, showing that the best agreement (minimum point) is achieved at λ_Δ. Thus, the EDR fits the data much better than the CDR: the SD σ_Δ between the experimental data and CDR is over 2.6 times larger (0.0377) than the deviation for EDR (0.0145), at $\lambda = \lambda_\Delta = 0.180$ mm^{-1}. This λ value does not necessarily equal λ_M, because it is derived from an entirely different binary graph measure. The similarity of these values indicates that the EDR captures important aspects of cortical network structure. In the following, unless specified otherwise, we used λ_Δ to generate the EDR graphs (0.150 mm$^{-1} = \lambda_{FLN} < \lambda_M < \lambda_\Delta < \lambda_d = 0.188$ mm^{-1}). Although the graphs are small (29 nodes) and the degree distributions noisy (Figures 4A and 4B), the comparisons between models and data nevertheless show that the EDR better captures the frequency distributions than does the CDR.

Prediction of Graph Spectra

Instead of comparing individual graph measures, we may evaluate a more stringent constraint by comparing the eigenvalue spectra of the networks generated by our models and the cortical network. The spectral decomposition of a graph on N nodes allows expressing its graph theoretical properties with the help of N eigenvalues and corresponding eigenvectors. While all graph measures can be expressed in a spectral form, for any particular graph measure, their specific spectral expressions may be difficult to obtain or may not have a particularly illuminating or intuitive form. However, if two eigenvalue spectra are similar, then most of the corresponding graph measures are also similar (two matrices connected by a similarity transformation have identical eigenvalues). This is what we examine next.

Let $\mathbf{A} = \{a_{ij}\}_{i,j=1}^{N}$ be the adjacency matrix of a graph $G(V, E)$ on N nodes, that is $a_{ij} = 1$ if nodes $i, j \in V$ are connected ($(i,j) \in E$) and $a_{ij} = 0$ otherwise. The set of eigenvalues $\theta_1 \geq \theta_2 \geq \ldots \geq \theta_N$ of $\mathbf{A}$ forms the spectrum of the graph $G(V, E)$ (Brouwer and Haemers, 2012; Chung, 1996). The eigenvalue spectrum of a graph is invariant, and it describes a wide range of local and global binary properties (Chung, 1996). In Figure 4C, we show a comparison between the spectra of graph eigenvalues (computed from the

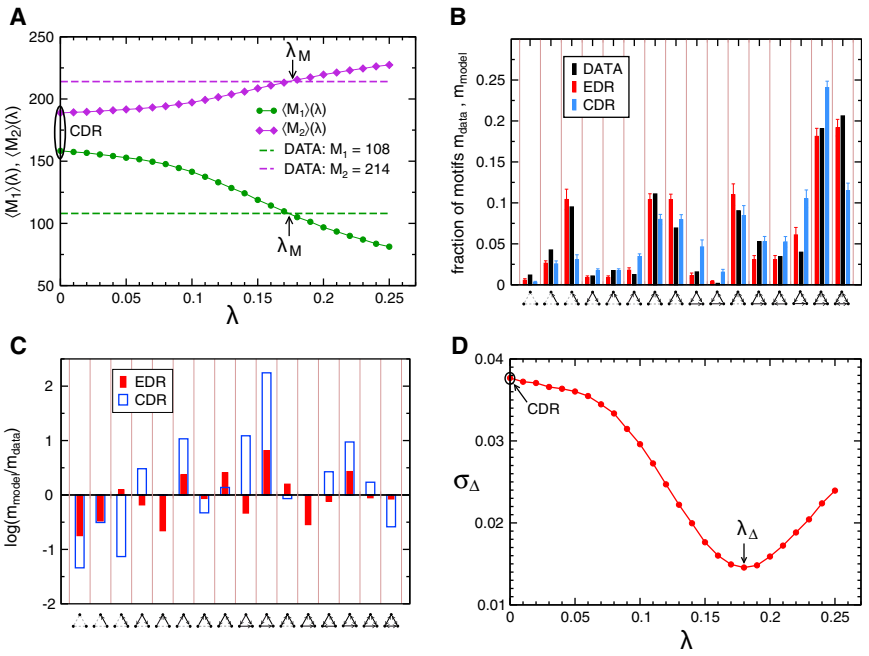

Figure 3. Distance Rules-Based Network Models of the Cortex

(A) The only model parameter λ here is set by setting the number of unidirectional links M_1 to that in the data (Markov et al., 2012).

(B) Motif fractions in the EDR and CDR models and data. Statistics were carried out on 1,000 random graph realizations; error bars show the SD.

(C) Logarithm of motif ratio counts between model and data.

(D) The SD of the deviations in (C) as function of λ, optimal agreement (minimum σ_Δ) is at $\lambda_\Delta = 0.180\ \mathrm{mm}^{-1}$.

adjacency matrix) and the same spectra of the model graphs, EDR and CDR. Since our graph G_{29x29} is directed, some of the eigenvalues will be complex. In Figure 4C, we show the absolute values $|\theta_i|$ of the eigenvalues for G_{29x29} and the averages of the eigenvalues after 200 realizations for both the CDR and EDR models. While both models closely capture most of the spectrum, the EDR does a better job. We expected the largest eigenvalue to be very close for G_{29x29} and the models because θ_1 is related to the average degree in the network, which was fixed by stopping the network growth in the models when they had as many binary connections as in the data. The second largest eigenvalue, however, is related to several important binary properties such as conductance and expansion properties and random walk mixing time. As Figure 4C shows, the EDR reproduces much better the second largest eigenvalue than does the CDR (the results are also similar if we look at the real and imaginary parts of the eigenvalues separately) and also the smallest eigenvalues (which are related to connectivity properties).

Predicting the Core Structure of the Cortex

There is evidence of core structures in cortical networks that are thought to play a role in functional integration (Hagmann et al., 2008; Harriger et al., 2012; Modha and Singh, 2010; van den Heuvel and Sporns, 2011). In our data, a strong indicator of the heterogeneity of the interareal cortical network at the binary level is revealed by a clique distribution analysis of the G_{29x29} graph. A *k*-clique is a complete subgraph of *k* nodes from G_{29x29} with all possible directed edges actually existing within this set of nodes (i.e., all $k(k-1)$ directed edges). The G_{29x29} graph's largest clique size is $k = 10$ and there are 13 such 10-cliques. While it is not unexpected to see large cliques in dense graphs, the appearance of 13 10-cliques is highly improbable even in a graph of 66% overall density (see below). The union of all areas participating in at least one of these 13 cliques is a set of 17 areas. There are 251 directed links within this set, which constitutes a very dense subgraph of density $\rho_{c-c} = 251/(17\times16)$ or 92% density. We refer to this set of 17 areas as the *high-density core*, or simply *core*, and to the set of remaining 12 nodes as the *periphery*. There are 220 links between the core and the periphery, corresponding to a density of $\rho_{c-p} = 220/(17\times12\times2)$ or 54% density. Finally, there are 65 directed edges linking the 12 nodes within the periphery, corresponding to a density of $\rho_{p-p} = 65/(12\times11)$ or 49% density. Since the G_{29x29} graph is edge complete, its entire set of links will stay the same following future tracer injections into additional areas. Thus, the density of 92% between these 17 nodes is the same within the FIN (G_{91x91}) itself. This implies that the FIN also has a high-density core that includes these 17 nodes (the full core might be larger). Figure 5A shows the 13 10-cliques and Figure 5B shows the 17-core as the superset of the 13 10-cliques. The white directed arrows in Figure 5B are the *missing links* in the core. Figure 6 shows on a flat-map the areas corresponding to the core and periphery (see Figure 6 for the 13 10-cliques on the same map).

To estimate the likelihood of such a core by chance, consider that the edges in the G_{29x29} were placed uniformly at random with a placement probability of p = 0.66 (from the density of G_{29x29}). The maximum number of edges between the 17 nodes listed in Figure 4B is 17 × 16 = 272. One can select in $\binom{272}{21}$ ways the 21 nonedges, each appearing with probability $(1-p)$. Thus, the probability that a specific set of 17 nodes has a density of 92% in a random graph is $\binom{272}{21}p^{251}(1-p)^{21} = 8.71\times10^{-25}$. The probability of a core of 17 (among any 17 nodes), obtained by multiplying the above number with the number of ways to select 17 nodes out of 29, is 4.52×10^{-17}, i.e., infinitesimal.

Figure 5C shows the distribution of cliques of various sizes in the data graph G_{29x29} compared with the same in the model graphs and a randomly rewired version of G_{29x29}, RAND. In the latter case, the rewiring preserved the degrees of all nodes by

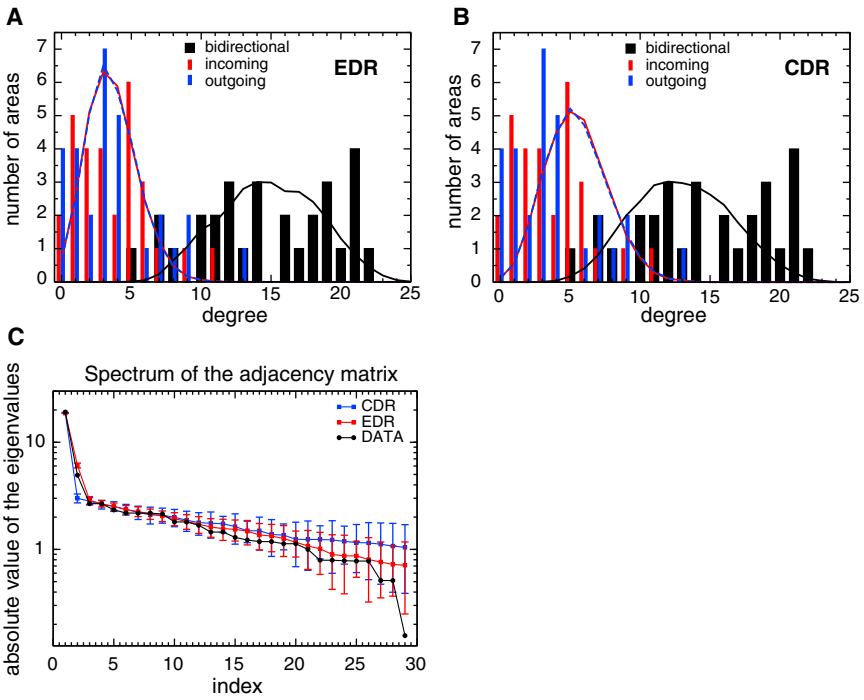

Figure 4. Prediction of Degree Distributions and Eigenvalue Spectra

(A and B) In- and out-degree distributions for unidirectional connections observed in data (red and blue bars, respectively) and the degree distribution for bidirectional connections (black bars). Curves: predictions of the two random graph models (CDR, EDR). EDR (A) better describes the experimental data than does the CDR (B), by capturing both the central tendency and the spread of the degrees.

(C) Absolute G_{29x29} graph spectra values for EDR and CDR models. Statistics were carried out on 200 random graph realizations; error bars show SD. Abscissa, i index of eigenvalue; ordinate, absolute value of the eigenvalue $|\theta_i|$.

edge swaps. This is much more restrictive than the simple random placement of links, and in this case, larger cliques occur more frequently but still well below those in G_{29x29}. Only the EDR model generates large cliques with high probability; both CDR and RAND produce practically zero values for 9- and 10-cliques (Figure 5C). The overall clique distribution is also much better matched by the EDR than by any of the other models. Thus, the strongly heterogeneous clique distribution (at the binary level) of the cortical network is also well recovered from the cost-of-wiring principle expressed in the exponential distance rule.

It is of interest to compare the weight distributions for the core, periphery, and core-periphery connections of G_{29x29}, rather than just the binary analysis described above. Figure 5D shows the FLN distribution within the core, within the periphery, and between core and periphery. Figure 5D shows that within the 17-core the links are mostly strong (the FLN distribution is skewed toward large FLN values, black circles) and as well among the nodes within the periphery. However, the edges connecting nodes between periphery and core are preponderantly weak (skewed toward small FLNs, blue circles). Interestingly, medium strength connections are found with almost equal distribution in all three substructures.

In summary, the binary properties of the G_{29x29} network are well captured by a random graph model based on the EDR. Although the binary network properties are based on the connections existing or not, they are nevertheless generated from a *continuous spatial property* of the system (distance rule). While the EDR is an averaged, biologically nonspecific rule, it expresses the strong economy around physical connection *lengths*, with higher costs associated with longer distances. This strongly determines cortical network structure. It might also influence the types of information theoretic algorithms the brain uses. In the next section, we explore how the range and distribution of weights and spatial geometry encode some of the specificity and functional structure of the cortical graph.

Communication Efficiency and the Backbone

The five orders of magnitude range of connection weights mean that information capacity is expected to vary differently along the high bandwidth within lobe pathways and the weak interlobe connections (Markov et al., 2013). To investigate how differences in connection strength shape the functional structure of the cortical graph, we approach the problem from a communication efficiency point of view. The f_{ij} can be interpreted as a measure of the capacity of information transfer between a source i and its target j. The higher f_{ij} (the stronger the projection), the higher the bandwidths of information transfer along the $i \rightarrow j$ link. Thus, to a first approximation, the probability for signals along the $i \rightarrow j$ link to induce activity in node k via the $j \rightarrow k$ link is proportional to the product $f_{ij}f_{jk} = \exp[\ln(f_{ij}) + \ln(f_{jk})]$. Therefore, it is more convenient to work with $w_{ij} = -\ln(f_{ij}) \geq 0$ as link weights, so that they are additive along directed paths. The w_{ij} is equivalent to link *resistance*, (larger w_{ij} means a weaker link or a higher resistance). For every pair of nodes (i,j), we define r_{ij} as the minimum sum of link weights (sum of w_{lk} weights taken along a path) among all paths directed from i to j. For constant weights, r_{ij} is proportional to the length (number of links) of the shortest directed path from i to j. We examined two communication efficiency measures, namely a global measure E_g (Latora and Marchiori, 2003) and a local measure E_l (Vragović et al., 2005).

The global network communication efficiency measure E_g introduced by (Latora and Marchiori, 2003) is defined as:

$$E_g = \frac{1}{N(N-1)} \sum_{i \neq j} \frac{1}{r_{ij}},$$

where the summation is over all the $N(N-1)$ possible pairs (i,j) of nodes. E_g is a global conductance measure for information transfer between two arbitrary nodes, calculated as the mean of the conductance $1/r_{ij}$ over all the $N(N-1)$ possible pairs.

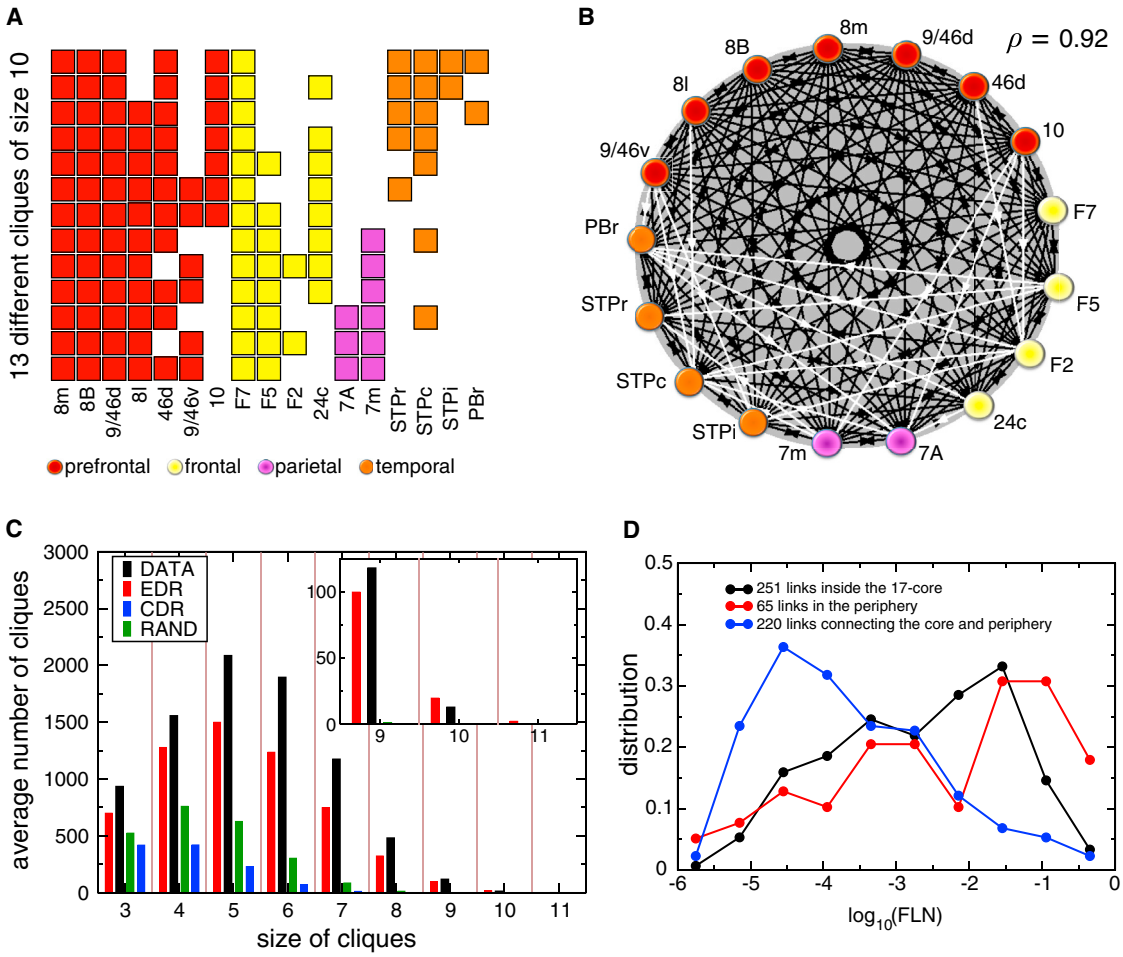

Figure 5. Core-Periphery Structure

(A) The 17 areas participating in the 13 10-clicks.

(B) White arrows, missing links between the 17 nodes of the core.

(C) Distribution of clicks, showing the average number of clicks of a given size in the model graphs (EDR, CDR), the degree-preserving randomly rewired graph (RAND), and the actual graph G_{29x29} (black). The averages were obtained from 10^3 realizations of the model graphs. The inset is a magnification of the corresponding region, showing that the EDR is the only model close to the value in the data.

(D) FLN distributions within the core-periphery structure of G_{29x29}. See also Figure S1.

The local network communication efficiency measure E_l introduced by (Vragović et al., 2005) is defined as:

$$E_l = \frac{1}{N}\sum_i \frac{1}{k_i(k_i-1)}\sum_{j\neq k\in\{i\}}\frac{1}{r_{jk/i}}.$$

Here a local efficiency is calculated for all pairs *j,k* of neighbors of node *i* after node *i* and its links are removed from the graph (obtaining $r_{jk/i}$ through the remaining graph), then this is averaged over all nodes *i*. The local efficiency is essentially the average conductance between all the areas connected to an area X, after removal of area X with its links (that is, through the rest of the network). It is similar to assessing how easily one can travel between the satellites of a town, without using routes passing through the town. Again, this is averaged across the entire graph.

We explored the role of the connection weights in communication efficiency, by simulating a threshold effect via progressively deleting the weakest links (green and blue solid lines, Figures 7A, 7B, and S2). The effect on global efficiency starts to decline sharply only after 76% of links (containing 5% of total neurons) have been removed. Hence, efficiency is assured by the remaining 24% of links exhibiting the largest FLN values and accounting for 95% of neurons. These links with the highest FLN assuring global efficiency have a mean projection distance of 16 mm (SD 8.4), considerably shorter than the 27 mm mean of the removed connections. This high FLN network constitutes the global efficiency (GE) backbone of the graph, shown in Figure 7E. This figure depicts a relative spatial placement of the areas that is optimal with respect to the weights, generated via the Kamada-Kawai (KK) force-based graph-drawing algorithm. In the final state, the areas (nodes) become clustered by the algorithm in a

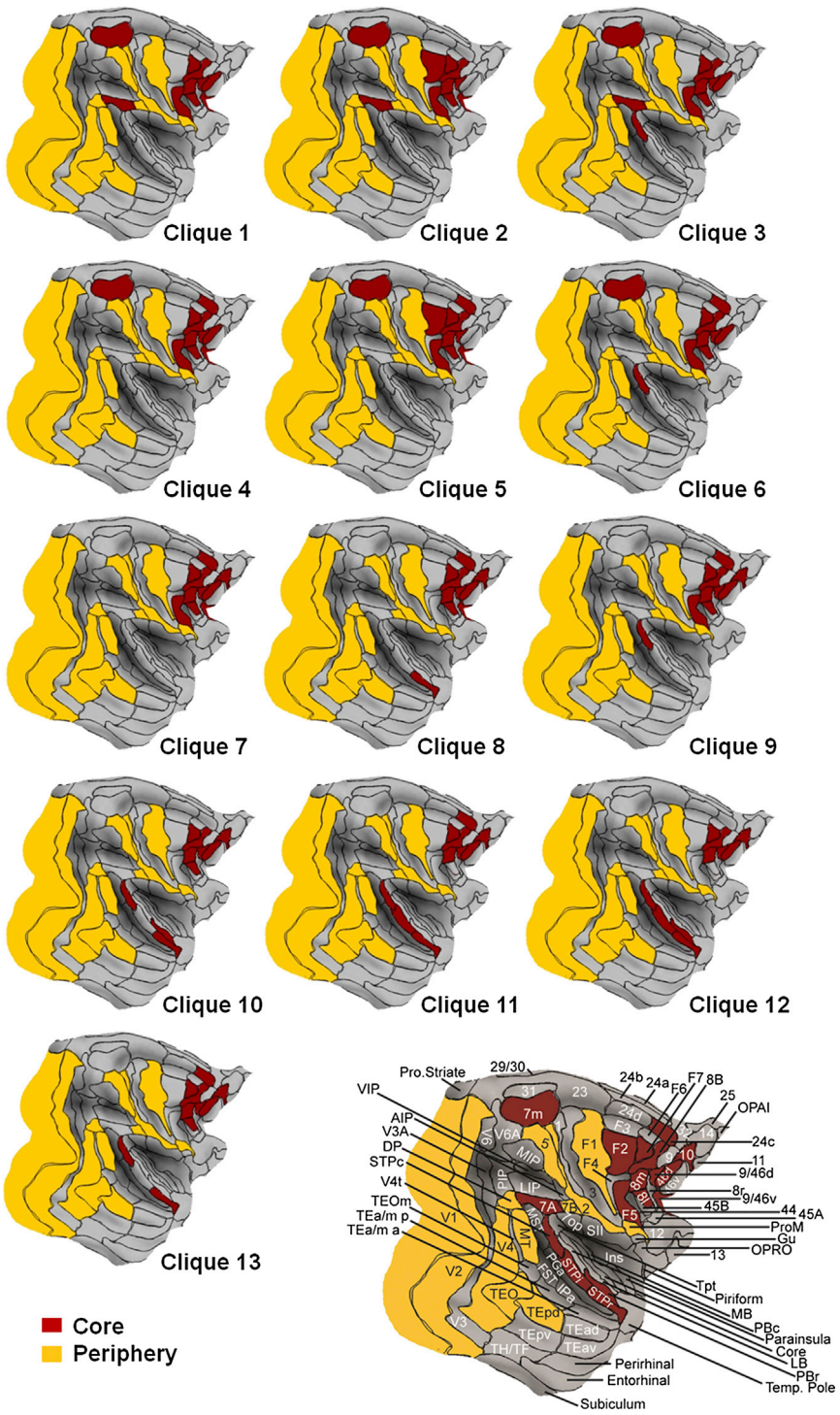

Figure 6. 2D Cortical Surface Map Localizing Core and Periphery

Areal members of the core are shown in red and of the periphery in yellow. See bottom right for areal names (see Markov et al., 2012 for abbreviations).

way to suggest their functional interactions. As more weak links are removed, regional groups of areas cluster in a connected network, forming a high-strength, high-bandwidth subgraph of the cortex.

Interestingly, with decaying density, global efficiency (green solid line in Figures 7A and 7B) remains virtually unchanged, while local efficiency (blue solid line) increases. The higher local, compared to global, efficiency suggests that local information processing is more voluminous and that within the clusters of areas in the backbone, the strong connections provide multiple alternative paths for functional interactions. Mathematically speaking, those terms increase in E_l for which the central node i loses a weakly connected neighbor j during the removal process. Due to the *distance rule*, however, if j is a weak link neighbor of i, then all its connections to the strong link neighbors of i must be weak, since j is then a node physically far from i and its immediate neighborhood (e.g., since Lyon is far from South Bend, it is also far from Chicago). Evidence that the differential effect of weak link removal is largely due to the distance rule is shown in Figures 7A and 7B. Both local and global efficiencies decay slowly for the CDR, whereas the EDR model displays a similar behavior as the data.

Wire Length Constraints

The architecture of cortical connectivity patterns is presumably scalable in order to accommodate the observed five orders of magnitude range in mammalian brain weight (Striedter, 2005). Adaptive changes in brain size pose specific design challenges for the neocortex, given the high cost of long-distance connections (Kaas, 2000). We, therefore, examined whether the spatial distribution of the cortical areas in the G_{29x29} network conforms to an optimal placement that minimizes total wire length.

The total wire length of a network depends on the positions of the nodes relative to each other and the number of links between node pairs. For a binary network, the total wire length is just the sum of the distances between existing links and will be referred to simply as the total distance or span. In the case of a weighted network, the total wire length is calculated as the sum over all edges of the product of the weight (FLN) and the projection distance. In the case of our network, each area is attributed to a point on the surface of the brain

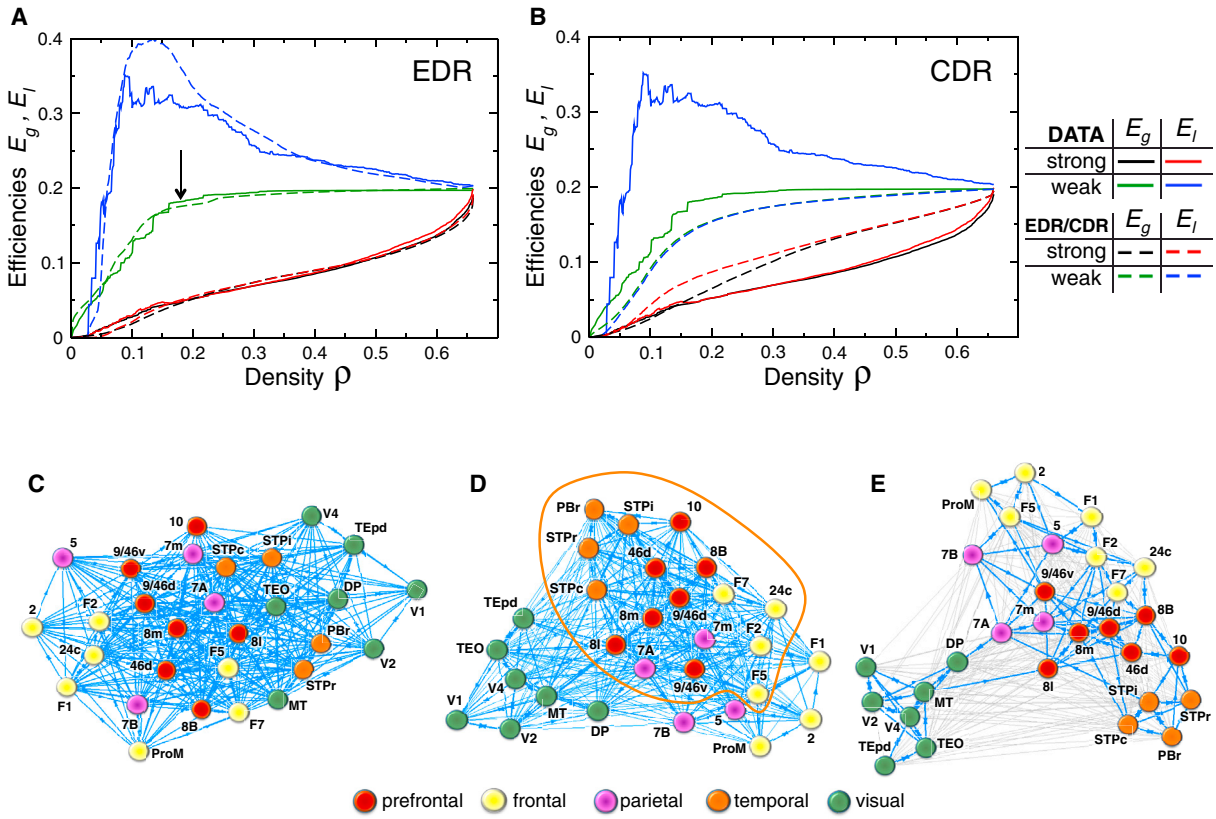

Figure 7. Global and Local Communication Efficiency

(A and B) Effects of graph density via sequentially deleting weak (blue, green) and strong (black, red) links. Data comparison with (A) EDR model, dashed lines and (B) CDR model, dashed lines.

(C–E) Weight-based layout and high-capacity backbone. Kamada-Kawaii, force-based graph-drawing algorithm reveals optimal layout. In this algorithm, links are springs with strengths proportional to the link weight. (C) Full density (all 536 links), all weights taken as unity (binary graph). (D) As in (C), with link weights given by their FLN values. Note the strong clustering by functional lobes. (E) Blue links, 130 strongest connections (0.16 density) left after weak link (thin gray) removal (indicated by the black arrow in A). The high-density core is encircled by the orange curve in (D). See also Figure S2. (See Supplemental Information for definitions.)

(i.e., in 3D space). We permuted the positions of the nodes of the network while preserving the connectivity pattern. This modifies the distance relations between the area and all of the other areas. We then performed optimization analyses in order to assess the influence of the positions of cortical areas on the total wire length of the network (see "Formalization of optimal placement" in Supplemental Information).

The total wire length for both the binary and weighted networks is smaller than that of every instance of a large sample ($p < 5 \times 10^{-6}$) of random permutations of the placement of areas in the network (Figure 8A). Global optimization algorithms used to search for an areal placement to minimize wire length revealed alternate organizations that shortened the binary network by no more than 5% (see Supplemental Information). For the weighted network, the only reductions found were small (<1%) and resulted from inversions of a few adjacent or nearby areas (Figure 8B). As the weight distribution is imposed by the EDR, we asked whether randomly generated EDR networks would optimize wire length. Figure 8C shows that the EDR generates networks that have total wire length that is 30% less than that of random permutations of the same network. In contrast, the CDR, on average, generates networks with no differences in wire length from that of their random permutations.

DISCUSSION

The network analyses have evolved into a widespread approach to characterizing key features of complex systems containing many interacting components. In spite of the fact that the primate cortex is one of the largest complex networks in existence, it has only recently been receiving appropriate attention (Sporns, 2011). Many earlier studies were based on incomplete data and are primarily descriptive characterizations using various graph theoretical measures, generating qualitative inferences concerning brain function. The present study is based on consistent and coherent brain-wide tracing data at the interareal level, aiming to provide a generative model with predictive capacity. The data were obtained from injections into 29 target areas distributed evenly across the cortex and revealed 1,615 pathways projecting into these targets from the 91 areas of the cortical parcellation, a third more than what has previously been identified (Markov et al., 2012). The projections among

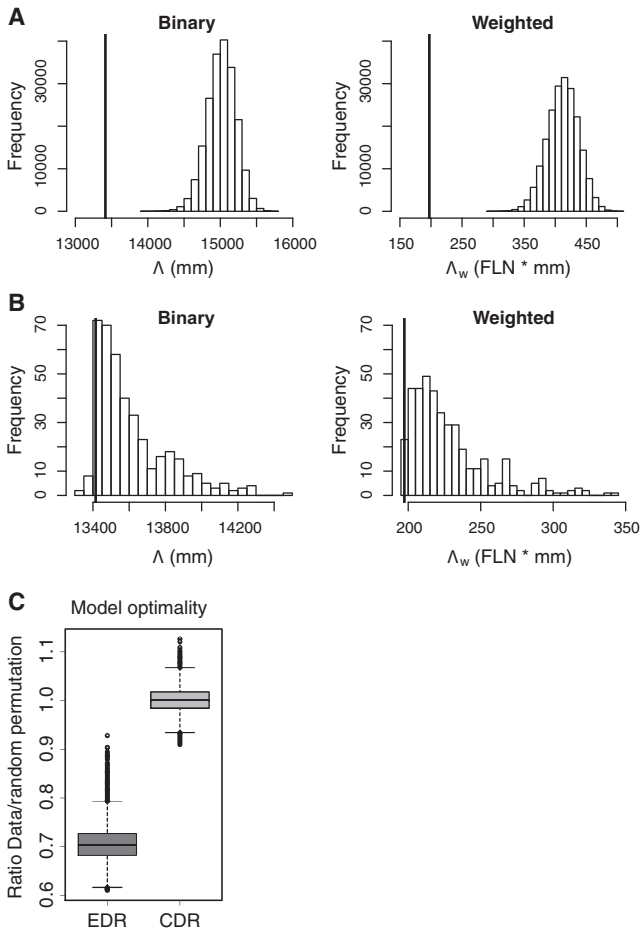

Figure 8. Wire Minimization

(A) Histograms of wire lengths (Λ) computed from 2 × 10^5 random node position permutations of the G_{29x29} for binary (left) and FLN-weighted (right) matrices. The wire lengths in the data shown as solid vertical lines. In each case, the wire length of the data is smaller than all random permutations.

(B) Histograms of wire lengths obtained from all 29 × 28/2 = 406 transpositions of pairs of areas from the G_{29x29} graph for the binary (left) and weighted (right) matrices. Solid vertical lines are as in (A). In the binary case, 27 transpositions lead to marginally shorter wire lengths, while for the weighted case there are only 3.

(C) For each of the 50 EDR and 50 CDR networks generated, we performed 2,000 random node permutations. Box plots of the ratios of the wire lengths for each of the 50 networks and their permutations show that EDR generates networks with 30% shorter wire lengths than a random permutation of the same network, while the CDR, on average, generates networks with no differences in wire length from their random permutations. The line in each box indicates median value. The error bars, the extreme data points that are no more than 1.5 times the interquartile range (approximately box height); the data points, values that are outside this range. See also Figures S3.

the 29 injected areas form an edge-complete subgraph of the FIN, i.e., it has complete connectivity information within this subset of 29 nodes. This edge-complete subgraph G_{29x29} is particularly useful, because incomplete data sets can introduce significant biases in analyses and conclusions (Kennedy et al., 2013). An example is the small-world (SW) hypothesis examined in earlier work claiming that the interareal network is sparse, exhibits short path lengths and high clustering, and that these properties form an organization principle of information integration in the cortex (Bassett and Bullmore, 2006; Bullmore and Sporns, 2012; Honey et al., 2007; Modha and Singh, 2010). In contrast, we find that the G_{29x29} is a very dense (66%) network; it is far from being sparse. A dominating set analysis shows that the FIN itself must be a dense graph as well (Markov et al., 2012). High-density graphs, however, generate short path lengths and high clustering "for free" in that these properties are not independent features of the system, as, for example, it would be in the social network (which has very low density, on the order of 10^{-7}), in which the SW property is a consequence of social behavior. Some of the conclusions drawn from incomplete data sets, however, can still be correct (qualitatively), such as those relating to the existence of a network core, but they are not assured.

The EDR Is a Major Determinant of Interareal Connectivity

The G_{29x29} revealed a strong heterogeneity in terms of interareal connection strengths obtained from the FLN, spanning five orders of magnitude and obeying a lognormal distribution (Markov et al., 2012). We have shown that the lognormal distribution of weights is a direct consequence of both the *physical constraint* of wiring costs appearing as the exponential decay of connection probability with distance and the geometrical constraint of the interareal distance distribution in the cortex. Interareal connection strengths represent a bandwidth measure for information transmission. Hence an information theoretic feature, i.e., the broad range of bandwidths, is generated via physical and structural means in the cortex. In order to explore the degree to which wiring costs and distance distributions determine both the binary and weighted properties of the interareal network, we introduced a simple random graph model based on these properties, which we call the exponential distance rule (EDR) model, expressing the cost of wiring principal in the cortex. Compared with a null model (CDR) that also uses the same distance distributions, but without the exponential cost to wiring, we were then able to determine the relative importance of the EDR in capturing the properties of the cortical network. Using a set of standard graph measures, we showed that the EDR performs much better than the CDR in capturing binary properties of the cortical data graph. Moreover, comparisons between the spectral properties of the model and data graphs demonstrate that the EDR is a strong determinant of the full set of structural properties of the cortical network.

Parameter Consistency of the Single-Parameter EDR Model

The unique parameter used in the EDR model is the decay rate λ. First, this rate λ can be determined directly from the empirical histogram of projection lengths, yielding $\lambda_d = 0.188\ \mathrm{mm}^{-1}$. Importantly, λ_d has nothing to do with network properties: it determines the probability of an interareal single neuronal projection to distance *d*. We then considered the empirical cortical data graph at the *binary* level (that is without any distance information in it, and simply based on the connections revealed by the injections). We used its properties to set the value of λ as a

parameter in the EDR model, by matching a binary property between the model network and the data graph. The simplest measure to match was the number of unidirectional connections, which generated a value of $\lambda_M = 0.174$ mm^{-1}, very close to λ_d obtained from physical distances alone. The next binary measure used was the distribution of motifs, which was best matched by the parametric EDR at $\lambda_\Delta = 0.180$ mm^{-1}. There is no reason why these estimates of the value of λ obtained from very different and independent criteria would be close to one another, unless the exponential cost to wiring is a strong determinant of the whole network structure.

Structural Heterogeneities

1. Cliques

A number of earlier studies have revealed highly connected regions in the cortex that share high degree and betweeness centrality, thereby constituting hubs with potentially important roles in promoting functional integration (Bassett et al., 2008; Hagmann et al., 2008). Hubs that form a larger number of mutual connections than would be predicted from the hub degree alone form a so-called rich club and are thought to exert an important control over the network (Colizza et al., 2006). In the cortex, a rich club subgraph has been shown by imaging studies to form an extensively connected network core, potentially playing an important role in integrating information (van den Heuvel and Sporns, 2011; Zamora-López et al., 2010; Zuo et al., 2012). Analysis of the density of connections linking the rich-club members suggests that they form a high-cost, high-capacity backbone for global cortical communication (van den Heuvel et al., 2012). The correlation of the rich club to regions of high metabolism further emphasizes the high cost of the rich club and points to a potential link with degenerative brain disorders (Bullmore and Sporns, 2012; Collin et al., 2013; Vaishnavi et al., 2010).

Previous studies using sparse connectivity data sets have used rich club (Colizza et al., 2006) and *k*-core analysis (Alvarez-Hamelin et al., 2005) methods to suggest the existence of a core-periphery *structure* of the macaque cortical network (Harriger et al., 2012; Modha and Singh, 2010). The G_{29x29} that we have explored has full connectivity information and is not biased by missing links within its set of 29 nodes. However, as the G_{29x29} graph is very dense, there are many high-degree nodes; the rich-club measure $\varphi_{norm}(k)$ is less sensitive than in strongly degree-heterogeneous sparse networks such as scale-free networks, for which it was introduced in the first place, and is unable to extract structure within the higher density subgraphs of an already dense graph (see Supplemental Information, "Rich-club analysis"). The *k*-core decomposition, based on thresholding by high-degree, is unable to identify structure within dense graphs, as the "core" identified this way will be formed by most of the nodes in the graph. Recall that even in the sparse 7% density graph of the Modha and Singh (2010) study, the core was formed by 31% of all nodes, already a large fraction. Thus, one needs a novel method that is better suited to extracting network cores from high-density graphs such as clique distribution analysis (Bron and Kerbosch, 1973). Our findings on the edge-complete part of our data corroborate the core existence and in addition show that such structures are strongly determined by the cost-of-wiring principle. The studies of Modha and Singh (2010) and Harriger et al. (2012) failed to include many weaker connections. Compared to a scale-free network, the G_{29x29} has many hub-like areas and an important aspect of their functions is their coalition to form a high-density core. There is good agreement overall between the present study and the two earlier studies showing that the prefrontal areas are strongly represented in the core structure of the cortex, coherent with the over abundance of prefrontal long-range connections (Markov et al., 2013) and the global neuronal workspace model of consciousness (Dehaene and Changeux, 2011). However, the core structure that we observe extends beyond the prefrontal cortex to include high-order associative areas in frontal, parietal, and temporal regions. It fulfills the requirements for a convergence-divergence-zone neural architecture, which has been suggested allows time-locked, multiregion activation required for perception and memory (Meyer and Damasio, 2009). Projections of core members to the periphery might mediate top-down processes such as control of attention (Miller and Buschman, 2013), employing rhythmic synchronization in order to facilitate communication between widespread areas (Fries, 2005; Gregoriou et al., 2012).

It is well accepted that brain networks achieve a cost-value tradeoff by minimizing the total wiring cost but retaining efficiency for integrative processing (Bullmore and Sporns, 2012). It has been argued that this tradeoff is achieved through the SW structure of cortical networks. However, given the high density of the cortical graph, it is more plausible that the tradeoff is achieved through the heterogeneous weight distribution resulting from the EDR. While many long-range connections exist providing good global efficiency, the wiring cost invested in these is much smaller due to the exponential decrease of the number of axons with their length (EDR). Additionally, we have shown that the existence of a dense core, believed to have a central role in generating globally efficient information flow, arises naturally from the EDR-based cost-value tradeoff.

2. The High-Efficiency Backbone

The unweighted (binary) edge-complete G_{29x29} graph displays some clustering that is mainly due to nodal degree (Figure 7C); the KK algorithm places the nodes with higher degree more centrally than the others. In contrast, the weighted edge-complete graph shows a stronger clustered network (Figure 7D) that becomes more pronounced in the GE backbone after pruning the weak links (Figure 7E).

The fact that weight heterogeneity is an organizational determinant of the embedded network has important implications. For instance, the capacity to shape the receptive fields in target areas is expected to be limited to broadband connections (Wang et al., 2010), which in the GE backbone are short range (Figure 7E). These broadband pathways will complement the communication of neighboring cortical areas via thalamic loops (Fries, 2009; Saalmann et al., 2012). One can speculate that the highly specific long-distance low-bandwidth connections between areas in different modules may coordinate activity via contraction dynamics (Wang and Slotine, 2005).

Because the high-weight links in the cortical network are restricted in distance, the constellation of areas of a given system constitutes a tightly knit community corresponding to a lobe or region. The high density of the connections of the global GE backbone linking the cortical areas in a defined region means

that these broadband connections exhibit little specificity. This contrasts with the long-distance, low-weight interlobe connections, which exhibit high specificity (Markov et al., 2013). These observations concerning the difference of the specificity of the within- and between-region connections are relevant to a recent percolation analysis of fMRI network obtained during dual task performance, showing that weak but specific links optimize global integration (Gallos et al., 2012a, 2012b).

Another feature that has been proposed as a byproduct of the SW property of the brain is the economical reconfiguration of functional networks in response to exogenous stimuli. Experiments have shown that during memory tasks requiring large cognitive efforts, magnetoencephalography networks show high efficiency while including a large proportion of long-distance edges (Kitzbichler et al., 2011). When cognitive demands are reduced, functional networks reconfigure to more modular structures with a smaller proportion of long-distance connections. Here we argue that the EDR naturally allows for this economical reconfiguration, and it is more relevant: when weaker links are not in use, the structure of the network is more modular (see Supplemental Information) and local communication efficiency greatly increases at the cost of only a slight decrease of the global efficiency. Moreover, the EDR graph model quantitatively captures this behavior observed in the data.

Total Wire Minimization

In contrast to an earlier study (Kaiser and Hilgetag, 2006) that examined optimal placement using an inconsistent database with a correspondingly low density and weights restricted to one of four possible ranks, we found that the G_{29x29} network does correspond to an optimized layout, confirming the findings of others (Cherniak, 2012; Klyachko and Stevens, 2003; Raj and Chen, 2011) (see Supplemental Information). This supports numerous studies showing that wire minimization is an important design constraint of the cortex (Cherniak, 1994, 2012; Cherniak et al., 1999, 2004; Chklovskii, 2000; Chklovskii and Koulakov, 2004; Chklovskii et al., 2002; Klyachko and Stevens, 2003; Koulakov and Chklovskii, 2001; Raj and Chen, 2011; Rivera-Alba et al., 2011). The EDR is the means by which the wire minimization principle is implemented since the random networks built with the EDR show optimal placement, whereas those built with the CDR do not (Supplemental Information). Elsewhere we have suggested that the lognormal distribution of FLN values could reflect the operation of a common rule governing axonal outgrowth in the cortex (Markov et al., 2011). During evolution, there is an increase in the number of cortical areas and the implementation of such a growth rule could provide an efficient way to generate near-optimal solutions to this NP-hard problem of combinatorial optimization of the areal layout during evolutionary time (Cherniak, 1994, 2012). Note that the spatial restriction of broadband connections means that increases in brain size is predicted to further increase isolation of clustered communities (Douglas and Martin, 2012; Herculano-Houzel et al., 2010).

The present findings show that the wire minimization constraint determines via the EDR the principal binary features of the cortical graph (including the motifs distribution, eigenvalue spectra, and the high-density core) and some of the weighted ones (lognormal distribution for the FLNs and the global and local efficiencies) as well as the gross brain morphology as reflected by folding of the cortical surface (Herculano-Houzel et al., 2010; Van Essen, 1997). The fact that the single-parameter EDR model captures the cortical network at so many levels suggests that the cortical network determined experimentally so far is not strongly influenced by noisy thresholding effects (see also the corresponding statistics analysis on inconsistency in Markov et al., 2012). Additionally, our efficiency analysis shows that the EDR describes the network properties of the data at all weight levels, as the sequential removal of the weakest links (both in the data and EDR) imposes varying thresholds on the graph (see Figure S2).

In summary, a simple, EDR-based random graph model captures quantitatively the structural specificity of the binary properties of the interareal network and explains the observed specificity of long-range connections (Markov et al., 2013). All real-world networks that perform a series of functions exhibit strong heterogeneity (Barabasi and Albert, 1999; Boccaletti et al., 2006; Newman, 2003; Watts, 1999a; Watts and Strogatz, 1998). In the cortex, this appears as a heavy-tailed distribution of the connection strengths spanning five orders of magnitude and conforming to a lognormal distribution. We have shown that this distribution is a direct consequence of the EDR and the spatial positioning of the areas and ensures wire minimization.

Interestingly, the structural features that we have described are found at different physical scales, insofar as interareal (long-range) connections share key properties with intrinsic (local) circuits. (1) Local connectivity, like interareal connectivity, shows an exponential decay in density (Markov et al., 2011) and reflects a decrease in the likelihood of synaptic contact with distance (Braitenberg and Schüz, 1998); (2) the lognormal distribution that is observed for interareal weights has also been found for the distribution of synaptic strengths of single neurons (Markov et al., 2012; Song et al., 2005; Wang et al., 2012); and (3) wire-length minimization applies to both interareal and local connectivity (Cherniak, 1994, 2012; Cherniak et al., 1999, 2004; Chklovskii, 2000; Chklovskii and Koulakov, 2004; Chklovskii et al., 2002; Klyachko and Stevens, 2003; Koulakov and Chklovskii, 2001; Laughlin and Sejnowski, 2003; Mitchison, 1991; Rivera-Alba et al., 2011). These parallels suggest that similar design principles may apply over multiple scales and conform to common requirements for constraint minimization.

EXPERIMENTAL PROCEDURES

Measurements of Interareal Distance

For a given pathway, source and target locations corresponded to geometric area centers (for V1, V2, and V4, see Supplemental Information). We evaluated the shortest physical distance between geometric centers through the white matter, thereby approximating axonal trajectories between areas. Weights and distances can be consulted at http://www.core-nets.org. A glossary is provided in Supplemental Information.

SUPPLEMENTAL INFORMATION

Supplemental Information includes Supplemental Experimental Procedures and three figures and can be found with this article online at http://dx.doi.org/10.1016/j.neuron.2013.07.036.

ACKNOWLEDGMENTS

We thank P. Giroud, P. Misery, L. Magrou, and A.R. Ribeiro Gomes for data analysis and B. Beneyton, M. Seon, and M. Valdebenito for animal husbandry. We thank C. Dehay, R. Douglas, K.A.C. Martin, W. Maass, and M. Cook for critical reading of the manuscript. This work was supported by FP6-2005 IST-1583 (H.K.); FP7-2007 ICT-216593 (H.K.); ANR-11-BSV4-501 (H.K.); LabEx CORTEX (ANR-11-LABX-0042) (H.K.), and in part by HDTRA 1-09-1-0039 (Z.T.), NIH R01-MH-60974 (D.C.V.E.), and by FP7-PEOPLE-2011-IIF-299915 (M.E.-R.).

Accepted: July 18, 2013
Published: October 2, 2013

REFERENCES

Aflalo, T.N., and Graziano, M.S. (2011). Organization of the macaque extrastriate visual cortex re-examined using the principle of spatial continuity of function. J. Neurophysiol. *105*, 305–320.

Alvarez-Hamelin, J.I., Dall'Asta, L., Barrat, A., and Vespignani, A. (2005). k-core decomposition: A tool for the visualization of large scale networks. arXiv, arXiv:cs/0504107, http://arxiv.org/abs/cs/0504107.

Bakker, R., Wachtler, T., and Diesmann, M. (2012). CoCoMac 2.0 and the future of tract-tracing databases. Front. Neuroinform. *6*, 30.

Barabasi, A.L., and Albert, R. (1999). Emergence of scaling in random networks. Science *286*, 509–512.

Barbas, H., and Rempel-Clower, N. (1997). Cortical structure predicts the pattern of corticocortical connections. Cereb. Cortex *7*, 635–646.

Bassett, D.S., and Bullmore, E. (2006). Small-world brain networks. Neuroscientist *12*, 512–523.

Bassett, D.S., Bullmore, E., Verchinski, B.A., Mattay, V.S., Weinberger, D.R., and Meyer-Lindenberg, A. (2008). Hierarchical organization of human cortical networks in health and schizophrenia. J. Neurosci. *28*, 9239–9248.

Boccaletti, S., Latora, V., Moreno, Y., Chavez, M., and Hwang, D.U. (2006). Complex networks: structure and dynamics. Phys. Rep. *424*, 175–308.

Bohland, J.W., Wu, C., Barbas, H., Bokil, H., Bota, M., Breiter, H.C., Cline, H.T., Doyle, J.C., Freed, P.J., Greenspan, R.J., et al. (2009). A proposal for a coordinated effort for the determination of brainwide neuroanatomical connectivity in model organisms at a mesoscopic scale. PLoS Comput. Biol. *5*, e1000334.

Boussaoud, D., Ungerleider, L.G., and Desimone, R. (1990). Pathways for motion analysis: cortical connections of the medial superior temporal and fundus of the superior temporal visual areas in the macaque. J. Comp. Neurol. *296*, 462–495.

Braitenberg, V., and Schüz, A. (1998). Cortex: Statistics and Geometry of Neuronal Connectivity, 2nd Edition. (Berlin: Springer-Verlag).

Bron, C., and Kerbosch, J. (1973). Algorithm 457: finding all cliques of an undirected graph. Commun. ACM *16*, 575–577.

Brouwer, A.E., and Haemers, W.H. (2012). Spectra of Graph. (New York: Springer).

Bullmore, E., and Sporns, O. (2012). The economy of brain network organization. Nat. Rev. Neurosci. *13*, 336–349.

Cherniak, C. (1994). Component placement optimization in the brain. J. Neurosci. *14*, 2418–2427.

Cherniak, C. (2012). Neural wiring optimization. Prog. Brain Res. *195*, 361–371.

Cherniak, C., Changizi, M., and Kang, D. (1999). Large-scale optimization of neuron arbors. Phys. Rev. E Stat. Phys. Plasmas Fluids Relat. Interdiscip. Topics *59*(5 Pt B), 6001–6009.

Cherniak, C., Mokhtarzada, Z., Rodriguez-Esteban, R., and Changizi, K. (2004). Global optimization of cerebral cortex layout. Proc. Natl. Acad. Sci. USA *101*, 1081–1086.

Chklovskii, D.B. (2000). Optimal sizes of dendritic and axonal arbors in a topographic projection. J. Neurophysiol. *83*, 2113–2119.

Chklovskii, D.B., and Koulakov, A.A. (2004). Maps in the brain: what can we learn from them? Annu. Rev. Neurosci. *27*, 369–392.

Chklovskii, D.B., Schikorski, T., and Stevens, C.F. (2002). Wiring optimization in cortical circuits. Neuron *34*, 341–347.

Chung, F.R.K. (1996). Spectral Graph Theory: CBMS Regional Conference Series in Mathematics, No. 92. (Providence: American Mathematical Society).

Colizza, V., Flammini, A., Serrano, M.A., and Vespignani, A. (2006). Detecting rich-club ordering in complex networks. Nat. Phys. *2*, 110–115.

Collin, G., Sporns, O., Mandl, R.C., and van den Heuvel, M.P. (2013). Structural and functional aspects relating to cost and benefit of rich club organization in the human cerebral cortex. Cereb. Cortex. Published online April 3, 2013. http://dx.doi.org/10.1093/cercor/bht064.

Dehaene, S., and Changeux, J.P. (2011). Experimental and theoretical approaches to conscious processing. Neuron *70*, 200–227.

Douglas, R.J., and Martin, K.A. (2012). Behavioral architecture of the cortical sheet. Curr. Biol. *22*, R1033–R1038.

Felleman, D.J., and Van Essen, D.C. (1991). Distributed hierarchical processing in the primate cerebral cortex. Cereb. Cortex *1*, 1–47.

Fries, P. (2005). A mechanism for cognitive dynamics: neuronal communication through neuronal coherence. Trends Cogn. Sci. *9*, 474–480.

Fries, P. (2009). Neuronal gamma-band synchronization as a fundamental process in cortical computation. Annu. Rev. Neurosci. *32*, 209–224.

Gallos, L.K., Makse, H.A., and Sigman, M. (2012a). A small world of weak ties provides optimal global integration of self-similar modules in functional brain networks. Proc. Natl. Acad. Sci. USA *109*, 2825–2830.

Gallos, L.K., Sigman, M., and Makse, H.A. (2012b). The conundrum of functional brain networks: small-world efficiency or fractal modularity. Front. Physiol. *3*, 123.

Gregoriou, G.G., Gotts, S.J., and Desimone, R. (2012). Cell-type-specific synchronization of neural activity in FEF with V4 during attention. Neuron *73*, 581–594.

Hagmann, P., Cammoun, L., Gigandet, X., Meuli, R., Honey, C.J., Wedeen, V.J., and Sporns, O. (2008). Mapping the structural core of human cerebral cortex. PLoS Biol. *6*, e159.

Harriger, L., van den Heuvel, M.P., and Sporns, O. (2012). Rich club organization of macaque cerebral cortex and its role in network communication. PLoS ONE *7*, e46497.

Herculano-Houzel, S., Mota, B., Wong, P., and Kaas, J.H. (2010). Connectivity-driven white matter scaling and folding in primate cerebral cortex. Proc. Natl. Acad. Sci. USA *107*, 19008–19013.

Honey, C.J., Kötter, R., Breakspear, M., and Sporns, O. (2007). Network structure of cerebral cortex shapes functional connectivity on multiple time scales. Proc. Natl. Acad. Sci. USA *104*, 10240–10245.

Jaynes, E.T. (1957). Information theory and statistical mechanics. Phys. Rev. *106*, 620–630.

Jouve, B., Rosenstiehl, P., and Imbert, M. (1998). A mathematical approach to the connectivity between the cortical visual areas of the macaque monkey. Cereb. Cortex *8*, 28–39.

Kaas, J. (2000). Why is brain size so important: design problems and solutions as neocortex gets bigger or smaller. Brain and Mind *1*, 7–23.

Kaas, J.H., and Collins, C.E. (2001). The organization of sensory cortex. Curr. Opin. Neurobiol. *11*, 498–504.

Kaiser, M., and Hilgetag, C.C. (2006). Nonoptimal component placement, but short processing paths, due to long-distance projections in neural systems. PLoS Comput. Biol. *2*, e95.

Kennedy, H., Knoblauch, K., and Toroczkai, Z. (2013). Why data coherence and quality is critical for understanding interareal cortical networks. Neuroimage *80*, 37–45, http://dx.doi.org/10.1016/j.neuroimage.2013.1004.1031.

Kitzbichler, M.G., Henson, R.N., Smith, M.L., Nathan, P.J., and Bullmore, E.T. (2011). Cognitive effort drives workspace configuration of human brain functional networks. J. Neurosci. *31*, 8259–8270.

Klyachko, V.A., and Stevens, C.F. (2003). Connectivity optimization and the positioning of cortical areas. Proc. Natl. Acad. Sci. USA *100*, 7937–7941.

Koulakov, A.A., and Chklovskii, D.B. (2001). Orientation preference patterns in mammalian visual cortex: a wire length minimization approach. Neuron *29*, 519–527.

Lanciego, J.L., and Wouterlood, F.G. (2011). A half century of experimental neuroanatomical tracing. J. Chem. Neuroanat. *42*, 157–183.

Latora, V., and Marchiori, M. (2003). Economic small-world behavior in weighted networks. Eur. Phys. J. B *32*, 249–263.

Laughlin, S.B., and Sejnowski, T.J. (2003). Communication in neuronal networks. Science *301*, 1870–1874.

Markov, N.T., Misery, P., Falchier, A., Lamy, C., Vezoli, J., Quilodran, R., Gariel, M.A., Giroud, P., Ercsey-Ravasz, M., Pilaz, L.J., et al. (2011). Weight consistency specifies regularities of macaque cortical networks. Cereb. Cortex *21*, 1254–1272.

Markov, N.T., Ercsey-Ravasz, M.M., Ribeiro Gomes, A.R., Lamy, C., Magrou, L., Vezoli, J., Misery, P., Falchier, A., Quilodran, R., Gariel, M.A., et al. (2012). A weighted and directed interareal connectivity matrix for macaque cerebral cortex. Cereb. Cortex. Published online September 25, 2012. http://dx.doi.org/10.1093/cercor/bhs1270.

Markov, N.T., Ercsey-Ravasz, M.M., Lamy, C., Ribeiro Gomes, A.R., Magrou, L., Misery, P., Giroud, P., Barone, P., Dehay, C., Toroczkai, Z., et al. (2013). The role of long-range connections on the specificity of the macaque interareal cortical network. Proc. Natl. Acad. Sci. USA *110*, 5187–5192.

Meyer, K., and Damasio, A. (2009). Convergence and divergence in a neural architecture for recognition and memory. Trends Neurosci. *32*, 376–382.

Miller, E.K., and Buschman, T.J. (2013). Cortical circuits for the control of attention. Curr. Opin. Neurobiol. *23*, 216–222.

Milo, R., Shen-Orr, S., Itzkovitz, S., Kashtan, N., Chklovskii, D., and Alon, U. (2002). Network motifs: simple building blocks of complex networks. Science *298*, 824–827.

Mitchison, G. (1991). Neuronal branching patterns and the economy of cortical wiring. Proc. Biol. Sci. *245*, 151–158.

Modha, D.S., and Singh, R. (2010). Network architecture of the long-distance pathways in the macaque brain. Proc. Natl. Acad. Sci. USA *107*, 13485–13490.

Mountcastle, V.B. (1998). The Cerebral Cortex. (Cambridge: Harvard University Press).

Newman, M.E.J. (2003). The structure and function of complex networks. SIAM Rev. *45*, 167–256.

Raj, A., and Chen, Y.H. (2011). The wiring economy principle: connectivity determines anatomy in the human brain. PLoS ONE *6*, e14832.

Ringo, J.L. (1991). Neuronal interconnection as a function of brain size. Brain Behav. Evol. *38*, 1–6.

Rivera-Alba, M., Vitaladevuni, S.N., Mishchenko, Y., Lu, Z., Takemura, S.Y., Scheffer, L., Meinertzhagen, I.A., Chklovskii, D.B., and de Polavieja, G.G. (2011). Wiring economy and volume exclusion determine neuronal placement in the Drosophila brain. Curr. Biol. *21*, 2000–2005.

Rockland, K.S. (1997). Element of cortical architecture: hierarchy revisited. In Extrastriate Cortex in Primates, K.S. Rockland, J.H. Kaas, and A. Peters, eds. (New York: Plenum Press), pp. 243–293.

Rosa, M.G., and Tweedale, R. (2005). Brain maps, great and small: lessons from comparative studies of primate visual cortical organization. Philos. Trans. R. Soc. Lond. B Biol. Sci. *360*, 665–691.

Saalmann, Y.B., Pinsk, M.A., Wang, L., Li, X., and Kastner, S. (2012). The pulvinar regulates information transmission between cortical areas based on attention demands. Science *337*, 753–756.

Schüz, A., and Miller, M. (2002). Cortical Areas: Unity and Diversity. (London: Taylor and Francis).

Song, S., Sjöström, P.J., Reigl, M., Nelson, S., and Chklovskii, D.B. (2005). Highly nonrandom features of synaptic connectivity in local cortical circuits. PLoS Biol. *3*, e68.

Sporns, O. (2011). Networks of the Brain. (Cambridge: MIT Press).

Sporns, O., Tononi, G., and Edelman, G.M. (2000). Theoretical neuroanatomy: relating anatomical and functional connectivity in graphs and cortical connection matrices. Cereb. Cortex *10*, 127–141.

Striedter, G.F. (2005). Principles of Brain Evolution. (Sunderland: Sinauer Associates).

Vaishnavi, S.N., Vlassenko, A.G., Rundle, M.M., Snyder, A.Z., Mintun, M.A., and Raichle, M.E. (2010). Regional aerobic glycolysis in the human brain. Proc. Natl. Acad. Sci. USA *107*, 17757–17762.

van den Heuvel, M.P., and Sporns, O. (2011). Rich-club organization of the human connectome. J. Neurosci. *31*, 15775–15786.

van den Heuvel, M.P., Kahn, R.S., Goñi, J., and Sporns, O. (2012). High-cost, high-capacity backbone for global brain communication. Proc. Natl. Acad. Sci. USA *109*, 11372–11377.

Van Essen, D.C. (1997). A tension-based theory of morphogenesis and compact wiring in the central nervous system. Nature *385*, 313–318.

Van Essen, D.C., and Ugurbil, K. (2012). The future of the human connectome. Neuroimage *62*, 1299–1310.

Vezoli, J., Falchier, A., Jouve, B., Knoblauch, K., Young, M., and Kennedy, H. (2004). Quantitative analysis of connectivity in the visual cortex: extracting function from structure. Neuroscientist *10*, 476–482.

Vragović, I., Louis, E., and Díaz-Guilera, A. (2005). Efficiency of informational transfer in regular and complex networks. Phys. Rev. E Stat. Nonlin. Soft Matter Phys. *71*(3 Pt 2A), 036122.

Wang, W., and Slotine, J.J. (2005). On partial contraction analysis for coupled nonlinear oscillators. Biol. Cybern. *92*, 38–53.

Wang, H.P., Spencer, D., Fellous, J.M., and Sejnowski, T.J. (2010). Synchrony of thalamocortical inputs maximizes cortical reliability. Science *328*, 106–109.

Wang, Q., Sporns, O., and Burkhalter, A. (2012). Network analysis of corticocortical connections reveals ventral and dorsal processing streams in mouse visual cortex. J. Neurosci. *32*, 4386–4399.

Watts, D.J. (1999a). Networks, Dynamics, and the small-world phenomenon. Am. J. Sociol. *105*, 493–527.

Watts, D.J. (1999b). Small Worlds: The Dynamics of Networks between Order and Randomness. (Princeton: Princeton University Press).

Watts, D.J., and Strogatz, S.H. (1998). Collective dynamics of 'small-world' networks. Nature *393*, 440–442.

Young, M.P. (1992). Objective analysis of the topological organization of the primate cortical visual system. Nature *358*, 152–155.

Zamora-López, G., Zhou, C., and Kurths, J. (2010). Cortical hubs form a module for multisensory integration on top of the hierarchy of cortical networks. Front. Neuroinform. *4*, 1.

Zeki, S. (2005). Introduction: cerebral cartography 1905-2005. Philos. Trans. R. Soc. Lond. B Biol. Sci. *360*, 651–652.

Zeki, S., and Shipp, S. (1988). The functional logic of cortical connections. Nature *335*, 311–317.

Zuo, X.N., Ehmke, R., Mennes, M., Imperati, D., Castellanos, F.X., Sporns, O., and Milham, M.P. (2012). Network centrality in the human functional connectome. Cereb. Cortex *22*, 1862–1875.